JOURNAL OF MATERIALS SCIENCE **39** (2004) 6221–6226

Contributions of the environmental scanning electron microscope and X-ray diffraction in investigating the structural evolution of a SiO_2 aggregate attacked by alkali-silica reaction

J. VERSTRAETE, L. KHOUCHAF
Centre de Recherche de l'Ecole des Mines de Douai, 941, rue Charles Bourseul BP. 838, 59508 DOUAI, France
E-mail: khouchaf@ensm-douai.fr

M. H. TUILIER
Equipe de Recherche Technologique, Université de Haute-Alsace, 61 rue Albert Camus, F-68093, Mulhouse Cedex, France

The structural changes of a flint aggregate attacked by alkali-silica reaction (ASR) were investigated using an environmental scanning electron microscope (ESEM) equipped with a X-ray microanalysis system. Compared to the conventional SEM, the ESEM enables the direct imaging of the samples in their natural state. The results obtained are compared to those acquired using X-ray diffraction (XRD). It appears that when calcium is present in the aggregate, the attack takes place from outside and progresses towards the inside of the aggregate. It has also been shown that calcium has an influence in slowing down the reaction by preventing the fast degradation of the aggregate. In addition, it supports the formation of new internal phases in the aggregate. The ESEM and XRD data were found to be consistent with each other.

1. Introduction

Most of the current advanced investigations concerning about the Alkali-Silica Reaction (ASR) effects within concrete use indirect methods and are limited to the study of the concrete regardless of the aggregate which is one of the main components in the concrete [1–3]. Observation of the ASR effects using Scanning Electron Microscope (SEM) is important because the attack of the aggregate is heterogeneous on the microscopic scale. One of the main problems in using the conventional SEM for the study of a concrete sample, is the requirement of sample preparation prior to imaging which may lead to an alteration of the true surface morphology or even the creation of artifacts. The ESEM solves these problems by permitting the direct imaging of the samples in their natural state [4–9].

ASR is a physicochemical process involving various components of concrete, including the siliceous phases containing SiO_2, the Ca^{2+} cations, and some alkaline K^+ and/or Na^+. The effects of ASR on the structure of concrete are detrimental. Several assumptions are usually made to explain the origins and the mechanisms of this reaction and its role in the degradation of concrete [10, 11]. In recent studies we evaluated the damage caused by ASR in a flint aggregate [12, 13], which enabled us determine some of the steps in the evolution of the crystal structure of the flint aggregate during the reaction. However, for an accurate explanation of the mechanism of degradation of concrete induced by ASR, it is necessary to observe the formation of new phases and their distribution inside or at the surface of the aggregate. In this study the flint aggregate has been analyzed in the ESEM in order to better understand the influence of each cation during ASR. Samples of this aggregate were subjected to the reaction: initially with calcium and potassium cation additions, and then with potassium additions only. X-ray diffraction was also used to characterize the aggregate. The results obtained from ESEM and X-ray diffraction are compared and discussed.

2. Materials and methods

The starting aggregate is a natural flint from the north of France. X-ray fluorescence analysis reveals a SiO_2 content close to 99.1%. XRD shows that it consists mainly of quartz with moganite traces. Sample preparation procedures and main steps of the ASR have been previously described [13, 14] but are briefly summarized here. The aggregate (1 g of crushed flint) was subjected to accelerated ASR at 80°C with a mixture of 0.5 g of portlandite $Ca(OH)_2$ and 10 ml of potash solution KOH at 0.79 mol/l (this system was labeled CaK); then another part of the aggregate was subjected to ASR with potash alone KOH (this system was identified K). The model reactor method used for the study

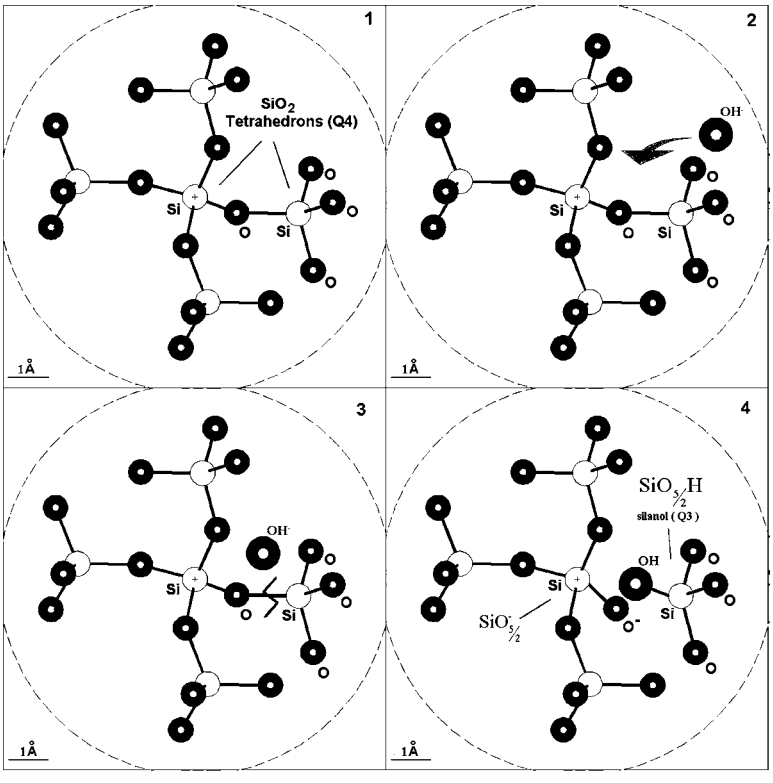

Figure 1 Schematic diagram showing the rupture of the Si─O─Si bonds by ASR.

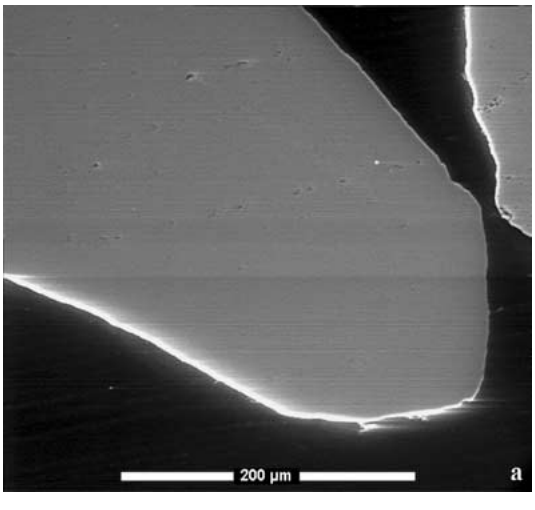

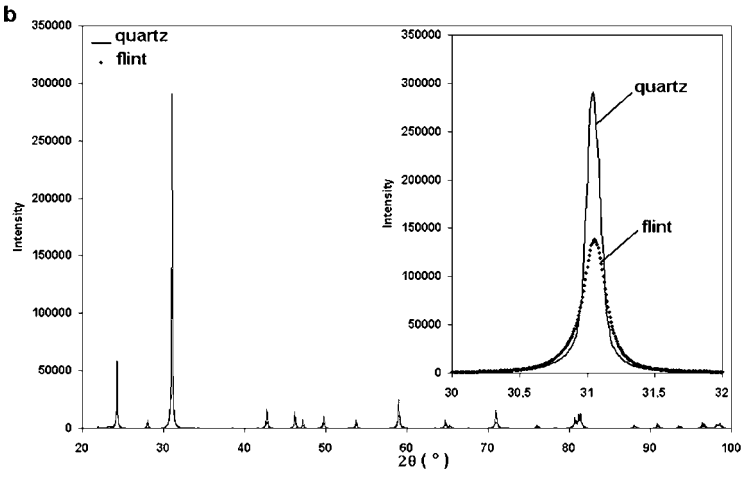

Figure 2 (a) ESEM micrograph of flint aggregate (GSED, 545.3 Pa) before ASR attack, (b) X-ray diffraction patterns of flint aggregate before ASR attack (·) and α-quartz (─).

was based on a section of the AFNOR P18-589 standard.

In the ASR mechanism, the hydroxyl, potassium and calcium ions contained in the solution within the concrete pores, penetrate poorly crystallized parts of the aggregate [15]. The attack is initiated by hydroxyl ions as shown below:

$$2SiO_2 + OH^- \leftrightarrow SiO^-_{5/2} + SiO_{5/2}H$$

inducing the rupture of Si─O─Si bonds between two tetrahedrons called Q_4 and producing negatively charged $SiO^-_{5/2}$ species and $SiO_{5/2}H$ species called silanols (see Fig. 1). The cations, which are abundant in the pores, are attracted to the sites of negative charge and participate in the reaction. The calcium cations are likely to react with silica species to form calcium silicate hydrate [15–17].

The observation was carried out on an ESEM Electro Scan 2020 equipped with an EDS Microanalysis system "Oxford Linkisis". The instrument has a tungsten filament and the accelerating voltage was 20 kV. The principle of operation and a more details of the experimental apparatus were reported by Khouchaf *et al*. [18]. The interest of the ESEM in many fields as well as its characteristics were largely discussed elsewhere, see for example Danilatos [4]. The use of the ESEM to observe the behavior of the flint aggregate during ASR is significant since our samples are insulating and any coating would involve problems with interpreting the images. In this study, the images were obtained using either gaseous secondary electron detector (GSED) or backscatterer electron detector (BSED).

X-ray diffraction data were obtained with a D8 Advance Bruker θ/θ diffractometer with monochromatic cobalt Co K_α radiation ($\lambda = 1.78897$ Å). The powder diffraction patterns were obtained between 10 and 100° (2θ) with a step size of 0.007° using a position sensitive detector (PSD) with a counting time of 10 s per step. The X-ray tube operated at 40 kV and 40 mA. α-quartz from NIST was used as a reference in XRD measurements.

3. Results and discussion

3.1. Flint aggregate

The image in Fig. 2a shows an area of the flint aggregate before ASR attack. The presence of well-defined geometrical grains which are characteristic of a polycrystalline material can be observed. Other images show the presence of randomly distributed pores sometimes reaching 3 to 5 μm. These images show a crystalline material with the presence of defects of structure. The structural defects within the aggregate are favorable sites for the ASR attack to start [15, 19]. For evaluating the structural quality of the flint aggregate, its XRD pattern was recorded and compared to that of α-quartz (Fig. 2b). The patterns reveal that all the peaks of α-quartz are present with a decrease in intensity. This feature confirms the observations by ESEM (Fig. 2a) which show the presence of defects within the flint. Indeed, the studies undertaken by Mehta and Monteiro [20] show a close connection between the crystallinity of a compound and its degree of reactivity. The presence of crystalline defects in the flint plays an important part in its behavior during the ASR.

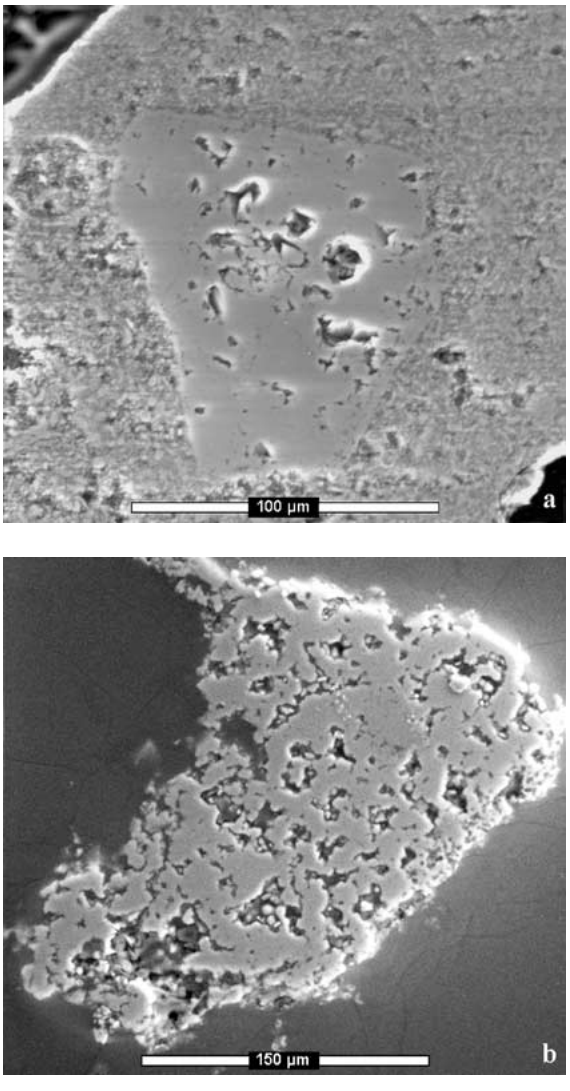

Figure 3 ESEM micrographs of (a) flint aggregate after 30 h of reaction (GSED, 532 Pa) and (b) flint aggregate after 168 h of reaction (BSED, 252.7 Pa) in (CaK) system.

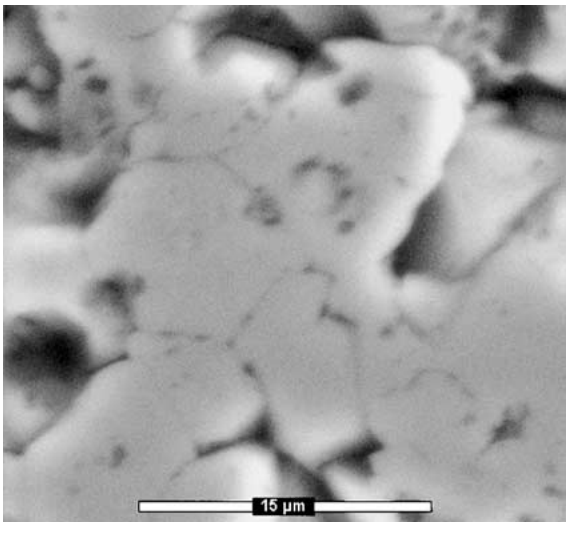

Figure 4 ESEM micrograph with zoom of flint aggregate after 168 h of reaction (BSED, 252.7 Pa) in (CaK) system.

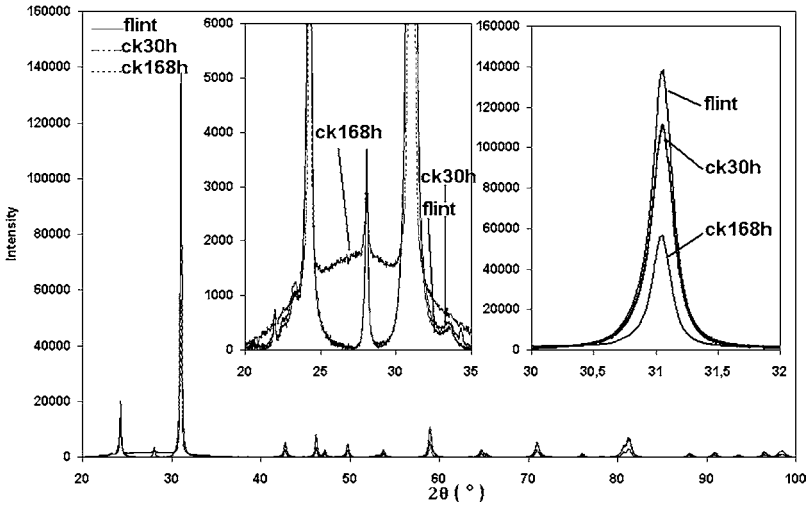

Figure 5 X-ray diffraction patterns in (CaK) system of flint aggregate (flint), flint aggregate after 30 h of reaction (ck30h), flint aggregate after 168 h of reaction (ck168 h).

3.2. (CaK) system

The flint was then subjected to attack by ASR. In (CaK) system, we observed that the degradation of the aggregate takes place both inside and at the surface of the aggregate. After 30 h of attack (Fig. 3a), the internal surfaces of the aggregate were heavily modified. First, it is interesting to note that the reaction has not proceeded to completion particularly in the center of the aggregate. The reaction begins at the outside regions progressing towards the inside in agreement with the work of Brouxel [1] and Rivard *et al*. [21]. Erosion due to the attack is observed on the surfaces as well as an increasing number of the holes inside the aggregate. Their size increases and varies between 20 and 38 μm. Some zones are attacked whereas others resist and remain similar to the initial flint. Moreover, less attacked zones have polygonal shapes. After 168 h of reaction (Fig. 3b), grains with better and worse-defined geometrical shapes appear. Even in this rather long term, the aggregate has not been completely affected.

Some grains observed with higher magnification are hexagonal (angle of 120°) (Fig. 4) with a diameter of approximately 10 μm. Areas with worse defined shapes are also observed and are attributed to amorphous and poorly crystallized silica in agreement with XRD results (Fig. 5) [13]. The hexagonal objects are thought to be SiO_2 quartz phases. Indeed, as the attack proceeds, the XRD patterns indicate a decrease in the intensities of the peaks and an increase in the vitreous diffuse halo located between 20° and 37° in 2θ (Fig. 5) which may be attributed to an increase in the fraction of the amorphous phase in the material [22, 23]. The irregular shapes present in Fig. 4 could be at the origin of this phenomenon. A decrease in the full width at half-maximum (FWHM) is also observed during the reaction. It varies between 0.17° in flint to 0.15° after 168 h of attack (in α-quartz FWHM is close to 0.09°). This reduction could be explained by the appearance of zones in which the degree of crystallinity is improving (Fig. 4). In addition, the formation and the evolution of amorphous and poorly crystallized phases could induce a variation of the volume of the aggregate and consequently participate in its swelling, which causes the rise of internal stresses in the concrete. Indeed, Grattan-Bellew *et al*. [3] have shown a correlation between the expansion of the concrete and the inverse of the particle size and surface area of quartz aggregate. To make such a correlation, the rate of expansion of mortar containing quartz with varying particle size was determined.

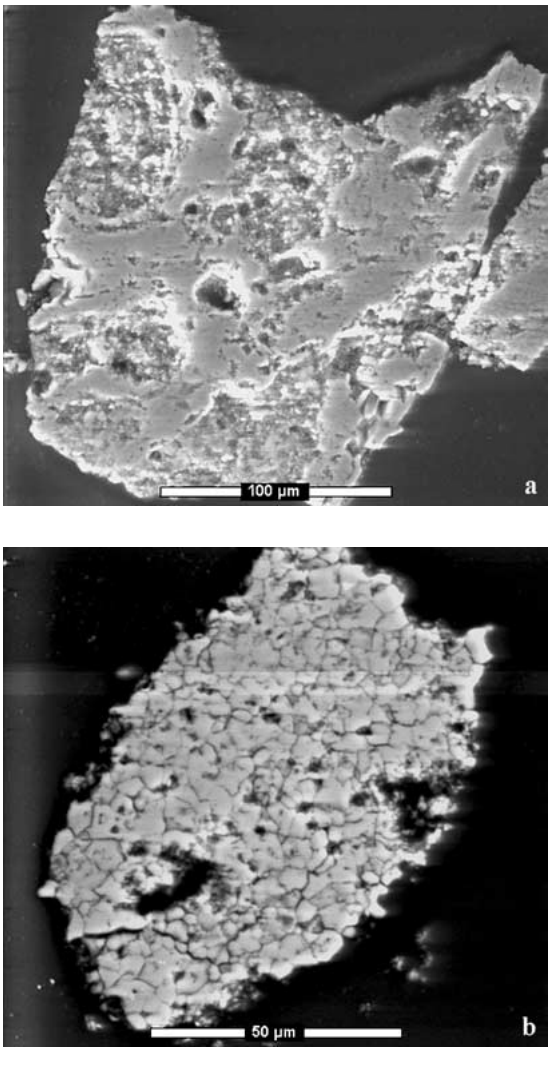

Figure 6 ESEM micrographs of (a) flint aggregate after 30 h of reaction (GSED, 558.6 Pa) and (b) flint aggregate after 168 h of reaction (GSED, 545.3 Pa) in (K) system.

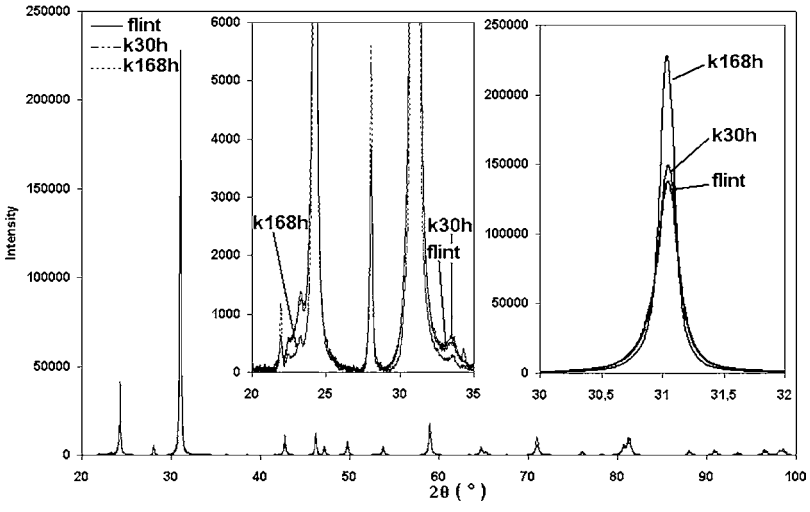

Figure 7 X-ray diffraction patterns of flint aggregate (flint), flint aggregate after almost 30 h of reaction (k30h), flint aggregate after 168 h of reaction (k168h).

In Fig. 4, it is important to note that the size of grains is very small compared to those observed at the beginning of the ASR. This means that the surface area of the aggregate increases and consequently the exposure of more internal defects open to the attack by ASR.

3.3. (K) system

In (K) system, it is noted that the degradation of the aggregate has been much faster (Fig. 6a). After almost 30 h of reaction, the attack appeared to be more advanced compared to the (CaK) system (Fig. 3a). Moreover, this attack did not follow a well defined direction as for the (CaK) system (Fig. 3a) where the reaction proceeds from the outside towards the inside of the aggregate. Other images with higher magnification reveal grains with better defined shapes. We point out that at this time, in the (CaK) system, well defined grains were not observed. The appearance of these crystalline shapes reveals an improvement of the crystallinity of the aggregate.

After 168 h of reaction, an increasing amount of zones with better geometric shapes can be seen, as well as a decrease in poorly defined zones (Fig. 6b). These features are in agreement with XRD results (Fig. 7). An improvement of the XRD patterns with an increase in the peaks intensities and a decrease in their FWHM compared to the one of the flint aggregate before ASR attack (the FWHM varies between 0.17° in flint to 0.11° after 168 h of attack).

These zones have smaller dimensions than the ones observed in the (CaK) system (Fig. 8). XRD patterns of the (K) system do not exhibit vitreous halos. This absence of halation (Fig. 7) and poorly defined zones on the images of Figs 6b and 8 show that in the (K) system the attack of the aggregate does not clearly induce the formation of amorphous phases which remain in the solid state in the product of the reaction as it is the case in the (CaK) system. Without calcium, the mechanism of the reaction could be summarized mainly into the dissolution of the aggregate, without the formation of internal products as occurs in the (CaK) system where the attack preferentially starts from the edge and progresses towards the inside of the aggregate as reported by Chatterji *et al*. [24], Wang and Gillot [25] and Prince and Perami [16]. After 168 h in (K) system, much better defined objects appear (Fig. 8). Between these objects remains no or less matter compared to (CaK) system. Indeed, in (K) system, the amorphous phase is dissolved into the liquid phase whereas in (CaK) system, this amorphous phase remains inside the aggregate which ensures the cohesion of the observed objects and the precipitation of new phases.

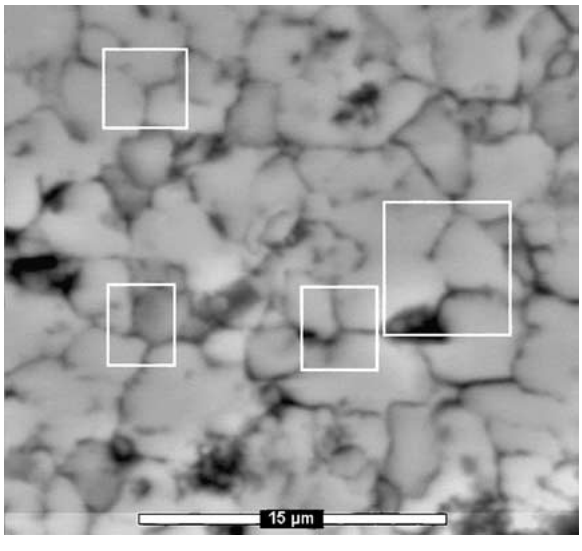

Figure 8 ESEM micrograph with zoom of flint aggregate after 168 h of reaction (GSED, 532 Pa) in (K) system.

4. Conclusions

This work provides an example of the usefulness of the ESEM in that it allows the structural changes in a flint aggregate affected by ASR to be followed directly. The particle size decrease observed by ESEM provides a good explanation of the observed reactivity increase during ASR. The results show that calcium has an influence in slowing down the reaction by preventing the fast degradation of the aggregate. In addition, it supports the suggestion that new phases form, which precipitate in the aggregate. The mechanism of

formation of the phases within the aggregate as well as their degree of crystallinity may provide a better explanation of the mode of expansion of concrete by the ASR which leads to its destruction. The results of ESEM and XRD were found to be consistent with each other. Finally it should be noted that this study could be extended to other aggregates. A study of the relationship between the obtained results and the local environment of silicon in the aggregate by X-ray absorption is under investigation.

Acknowledgments

Authors would like to thank Dr. D. Bulteel for his help in preparing the samples.

References

1. M. BROUXEL, *Cem. Concr. Res*. **23** (1993) 309.
2. P. FAUCON, J. M. DELAYE, J. VIRLET, J. F. JACQUINOT and F. ADENOT, *ibid.* **27**(10) (1997) 1581.
3. P. E. GRATTAN-BELLEW, J. J. BEAUDOIN and V.-G. VALLÉE, *ibid.* **28**(8) (1998) 1147.
4. G. D. DANILATOS, in "Fundations of Environmental Microscopy" (Advances in Electronics and Electron Physics, Academic Press Inc., 71, 1988) p. 109.
5. M. E. TAYLOR and S. A. WIGHT, *Scanning* **18** (1996) 483.
6. C. M. NEUBAUER, T. B. BERGSTROM, K. SUJATA, Y. XI, A. J. GARBOCZI and H. M. JENNINGS, *J. Mater. Sci.* **32** (1997) 6415.
7. W. JIANG, M. R. SILSBEE and D. M. ROY, *Cem. Concr. Res*. **27**(10) (1997) 1501.
8. G. GILLEN, S. WIGHT, D. BRIGHT and T. HERNE, *Scanning* **20** (1998) 404.
9. M. MOURET, A. BASCOUL and G. ESCADEILLAS, *Cem. Concr. Res.* **29** (1999) 369.
10. A. B. POOLE, in Proceedings of the 9th International Conference on Alkali-Aggregate Reaction (Concrete Society Publications CS 104, 1, London, England, 1992) p. 782.
11. S. CHATTERJI and N. THAULOW, in Proceedings of the 11th International Conference on Alkali-Aggregate Reaction in Concrete, edited by M.A. Berube *et al*. (Quebec, Canada, 2000) p. 21.
12. D. BULTEEL, E. GARCIA-DIAZ, J. DÜRR, L. KHOUCHAF, C. VERNET and J. M. SIWAK, *J. Phys. IV* **10** (2000) 513.
13. J. VERSTRAETE, L. KHOUCHAF, D. BULTEEL, E. GARCIA-DIAZ, A. M. FLANK and M. H. TUILIER, *Cem. Concr. Res.* **34** (2004) 581.
14. D. BULTEEL, E. GARCIA-DIAZ, C. VERNET and H. ZANNI, *ibid.* **32** (2002) 1199.
15. K. E. KURTIS, P. J. M. MONTEIRO, J. T. BROWN and W. MEYER-ILSE, *ibid.* **28**(3) (1998) 411.
16. W. PRINCE and R. PERAMI, *ibid.* **23**(5) (1993) 1129.
17. M. PREZZI, P. J. M. MONTEIRO and G. SPOSITO, *ACI Journal* **94** (1997) 10.
18. L. KHOUCHAF and J. VERSTRAETE, *J. Phys. IV* **12** (2002) 341.
19. LIANG TONG, MEIHUA WANG, SUFEN HAN and MINGSHU TANG, *Adv. Cem. Res.* **9**(34) (1997) 55.
20. P. K. MEHTA and P. J. M. MONTEIRO, in "Concrete: Structure, Properties, and Materials" (Prentice Hall, Englewood Cliffs, New Jersey, 1993).
21. P. RIVARD, J. P. OLLIVIER and G. BALLIVY, *Cem. Concr. Res.* **32**(8) (2002) 1259.
22. H. P. KLUG and L. E. ALEXANDER, in "X-ray Diffraction Procedures for Polycrystalline and Amorphous Materials" 2nd printing (John Wiley & Sons, Inc., New York, 1959) p. 586.
23. M. CYR, B. HUSSON and A. CARLES-GIBERGUES, *J. Phys. IV* **8** (1998) 23.
24. S. CHATTERJI, A. D. JENSEN, N. THAULOW and P. CHRISTENSEN, *Cem. Concr. Res.* **16** (1986) 246.
25. H. WANG and J. E. GILLOT, *ibid.* **21** (1991) 647.

Received 18 August 2003
and accepted 11 May 2004